Understanding the influence of 3D sidewall roughness on observed line-edge roughness in scanning electron microscopy images

Van Kessel, L.; Huisman, T.; Hagen, C. W.

DOI
10.1117/12.2550240

Publication date
2020

Document Version
Final published version

Published in
Proceedings of SPIE

Understanding the influence of 3D sidewall roughness on observed line-edge roughness in scanning electron microscopy images

van Kessel, L., Huisman, T., Hagen, C.

L. van Kessel, T. Huisman, C. W. Hagen, "Understanding the influence of 3D sidewall roughness on observed line-edge roughness in scanning electron microscopy images," Proc. SPIE 11325, Metrology, Inspection, and Process Control for Microlithography XXXIV, 113250Z (20 March 2020); doi: 10.1117/12.2550240

SPIE.

Event: SPIE Advanced Lithography, 2020, San Jose, California, United States

Understanding the influence of 3D sidewall roughness on observed line-edge roughness in scanning electron microscopy images

L. van Kessel[a], T. Huisman[b], and C.W. Hagen[a]

[a]Delft University of Technology, Dept. Imaging Physics, Lorentzweg 1, 2628 CJ Delft, The Netherlands
[b]ASML Netherlands B.V., De Run 6501, 5504 DR Veldhoven, The Netherlands

ABSTRACT

Line-edge roughness (LER) is often measured from top-down critical dimension scanning electron microscope (CD-SEM) images. The true three-dimensional roughness profile of the sidewall is typically ignored in such analyses.

We study the response of a CD-SEM to sidewall roughness (SWR) by simulation. We generate random rough lines and spaces, where the SWR is modelled by a known power spectral density. We then obtain corresponding CD-SEM images using a Monte Carlo electron scattering simulator. We find the measured LER from these images, and compare it to the known input roughness.

We find that, for isolated lines, the SEM measures the outermost extrusion of the rough sidewall. The result is that the measured LER is up to a factor 2 less than the true on-wafer roughness. The effect can be accurately modelled by making a top-down projection of the rough edge. Our model for isolated lines works fairly well for a dense grating of lines and spaces, as long as the trench width exceeds the line height.

Keywords: Scanning electron microscopy, Line edge roughness, Sidewall roughness, Metrology, Monte Carlo methods

1. INTRODUCTION

As lithography techniques move towards smaller and smaller features, line-edge roughness (LER) becomes an increasingly important parameter. Consequently, accurate metrology of LER has generated plenty of interest in recent years.[1–3]

LER is usually measured from top-down critical dimension scanning electron microscope (CD-SEM) images. As CD-SEM is a two-dimensional imaging technique, the profile along the vertical direction is not easily accessible. Most studies of LER metrology by SEM therefore ignore the 3D roughness profile along the sidewall's vertical direction. In this work, we will use the term LER when referring to the roughness of the measured line profile in a CD-SEM image. Sidewall roughness (SWR) will refer to the physical roughness of the on-wafer profile.

SWR can be measured by, for example, tilted or cross-section SEM, or atomic force microscopy (AFM). Thick resist films exhibit near-isotropic SWR after development.[4,5] Strong anisotropy is typically observed after etch.[4,6,7] Thin resists used for recent technology nodes show strong anisotropy with striations in the vertical direction.[8,9]

The influence of SWR on CD-SEM images has been experimentally investigated by Foucher *et al.*[5,10] and Fouchier *et al.*[11,12] These experimental studies show that 3σ LER measured from CD-SEM can be significantly less—by more than a factor 2—compared to the 3σ SWR measured by AFM*.

E-mail: L.C.P.M.vanKessel@tudelft.nl
E-mail: Thomas.Huisman@asml.com
E-mail: C.W.Hagen@tudelft.nl

*Fouchier *et al.*[11,12] conclude that the LER measured by CD-SEM matches the SWR measured by AFM very well, if the roughest upper layers of the feature are discarded from the AFM data. However, it is likely that the SEM is most sensitive to the upper layers, in which case figure 8 from Ref. 11 indicates the difference could be a factor 2.

Metrology, Inspection, and Process Control for Microlithography XXXIV, edited by Ofer Adan, John C. Robinson, Proc. of SPIE Vol. 11325, 113250Z · © 2020 SPIE
CCC code: 0277-786X/20/$21 · doi: 10.1117/12.2550240

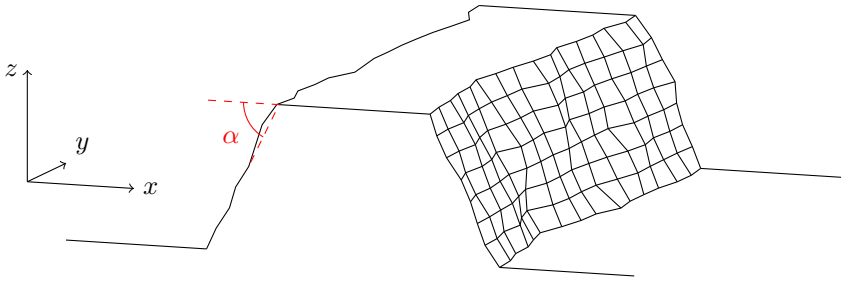

Figure 1. Sketch of the line profile studied in this work. We start with a trapezoidal structure. The sidewalls are randomly displaced by a roughness model, while the top and substrate remain flat. Also shown is our choice of coordinate system and definition of sidewall angle α. In the main text, we only consider lines with $\alpha = 90°$. Different sidewall angles are used in appendix A.

Simulation studies have also been performed.[13–15] These studies start with a known geometry and obtain corresponding CD-SEM images using full electron scattering simulations. These simulation studies all confirm that the measured 3σ LER can be up to a factor 2 less than the true 3σ SWR. However, none of them attempt to explain where this bias comes from, or how the measured power spectral density (PSD) corresponds to the true physical PSD.

In this study, we model the most dominant effect for the bias between LER and SWR, and show how the observed PSD is related to the physical PSD. We do this by simulation. We generate line-space patterns with random rough sidewalls using a model PSD. We then obtain corresponding top-down SEM images using a Monte Carlo electron scattering simulator. We find the measured LER by extracting the contours from these images, computing the measured PSD and subtracting the white noise floor. This unbiased measured roughness can then be compared to the input roughness.

The method of generating random features, simulating a SEM image, and extracting contours, is described in section 2. We first show results for the simple case of no roughness in the vertical direction in section 3. In section 4, we move to isolated lines with 3D roughness. Dense line-space patterns are studied in section 5.

2. METHOD

We study a pattern of lines and spaces in resist. We start with perfectly trapezoidal lines. The sidewalls are always vertical, except in appendix A. The sidewalls of these lines are then modulated by random roughness according to a model PSD (section 2.1). To guarantee that the geometry never self-intersects, there is no roughness on top of the lines. The situation is sketched in figure 1. A more complete study should include top and bottom corner rounding, and have roughness everywhere.

We then use a simulator of electron-matter interaction (section 2.2) to obtain the corresponding SEM image. Contours are extracted from this image using a thresholding method (section 2.3). The resulting measured power spectrum can then be compared to the known input PSD.

The resist lines are made of PMMA, the substrate is silicon. We have performed the same study with silicon lines on a silicon substrate, with very similar results. This gives confidence that the results are general: they are dominated by the geometry of the sample and not material contrast.

2.1 Generation of Rough Features

We use the method of Thorsos[16] to generate rough sidewalls. As explained by Mack,[17] the variance of the data produced by this method is biased compared to the intended value. Additionally, because the roughness is periodic, the shape of the PSD is biased if the length of the feature is on the order of the correlation length.

The bias is small when $\Delta x \ll \xi \ll L$, where Δx is the grid spacing, ξ is the correlation length of the roughness spectrum, and L is the total size of the domain. In the direction along the line, this requirement is automatically satisfied by our choices of Δx, ξ and L. In the vertical direction, however, it is often the case that ξ is close to L or larger. Our solution is to use the Thorsos method to generate much higher sidewalls than required, and using

only a section of the desired size. After this step, the generated PSD closely follows the intended profile. Any remaining bias between the target and true 3σ SWR is small, but we subtract the mean and scale the amplitudes to guarantee that the 3σ SWR is exactly as intended.

We use the following model PSD:

$$PSD(f_y, f_z) = \frac{4\pi H \xi_y \xi_z \sigma^2}{\left[1 + (2\pi f_y \xi_y)^2 + (2\pi f_z \xi_z)^2\right]^{H+1}}. \tag{1}$$

This is the PSD suggested by Palasantzas,[18] modified to allow for different correlation lengths ξ_y and ξ_z in the y and z directions, respectively. H is the Hurst exponent, which is the same in all directions, and σ is the root-mean-square roughness. f is the spatial frequency, 1/wavelength.

The one-dimensional version of this PSD is given by

$$PSD(f) = \frac{\Gamma(H + \frac{1}{2})}{\Gamma(H)} \frac{2\sqrt{\pi}\xi\sigma^2}{\left[1 + (2\pi f \xi)^2\right]^{H+1/2}}, \tag{2}$$

where $\Gamma(x)$ is the gamma function.

2.2 SEM Simulator

SEM images are simulated using a Monte Carlo electron tracing method. Electrons can undergo three types of scattering: elastic, in which electrons are deflected but keep their energy; inelastic, in which electrons lose energy and may create a secondary electron; and boundary crossing.

Elastic scattering is described by Mott scattering, calculated by solving the Dirac equation in a model potential around an atom. We use the ELSEPA program[19] to compute these cross sections. At low energies ($< 100\,\text{eV}$), we transition to electron–acoustic phonon scattering, as described by Schreiber and Fitting.[20]

Inelastic scattering is described by a dielectric function model. We use measured optical data,[21] extended to nonzero momentum by the full Penn algorithm.[22] Our numerical implementation follows the description of Shinotsuka *et al.*[23]

Finally, near a material interface, an electron may be either reflected or transmitted and refracted due to the difference in inner potential. We use a simple quantum mechanical step function model to determine these coefficients.

Our simulator runs on graphics cards using the method of Verduin *et al.*[24] to allow a large-scale simulation study. A typical simulation run, with more than 10 million triangles making up the rough line geometry and more than 200 million primary electrons at 300 eV landing energy, takes less than 10 minutes on an Nvidia GTX1080.

2.3 Contouring Method

A large variety of contouring methods is available in the literature. The reason why this large variety exists is that a simple thresholding method is plagued by robustness issues due to SEM noise. Filtering solves the robustness issue, but filters along the direction of the line must be avoided because they inevitably also affect the LER signal.

Alternative methods based on fitting reference linescan models[25,26] do not rely on filtering or a threshold, and work well even for very noisy images. However, such methods assume that the linescan—and with it, the sidewall's vertical profile—is the same for every position along the line. The applicability of these methods has not yet been proven for features with SWR, and therefore, we do not use such a method.

We opted for a simple thresholding method, with minimal filtering to make it robust. We have set the threshold to 60% between the minimum and maximal signal of every linescan. This value does not significantly influence our results, unless the feature has a sidewall angle or the trenches are narrower than the height of the lines. These situations are further discussed in appendix A. We use a $\sigma = 1\,\text{nm}$ Gaussian blur in the direction

perpendicular to the line. Note that this filter does not operate along the line, and hence does not affect the measured PSD.

Despite this, the SEM signal in a linescan may cross the threshold multiple times. Only when the slope is as expected (*i.e.* positive for a left edge, negative for a right edge) do we consider a threshold crossing as a candidate for edge detection. In the exceedingly rare case that there are still multiple candidates, we select the one closest to the mean edge position.

Because this is a simulation study, we can make the noise levels in the SEM images arbitrarily low. We have used 100 electrons per pixel, and disabled Poisson shot noise from the electron source. This gives images that are less noisy than those from a real CD-SEM. In reality, due to shrinking and charging effects, one should use much lower doses when acquiring a SEM image. A more sophisticated contouring algorithm is then required.

We now have a set of measured edge positions, one for each edge in the image. The PSDs for each of these edges can be determined and averaged. Though the contouring method always finds a reasonable edge position, it remains sensitive to statistical noise of the SEM. Assuming that the noise is uncorrelated from pixel to pixel, this manifests itself as a white "noise floor", which can be subtracted from the measured PSD.[3,27]

If the noise floor is very low, the measured PSD is not always completely flat at high frequencies. We measure the height of the floor by fitting the function

$$PSD(f) = a\, f^{-b}\, e^{-cf^2} + d \tag{3}$$

on a log-scale to the highest half of the frequencies. The f^{-b} term represents the typical power-law behaviour at high frequencies. The e^{-cf^2} term accounts for possible additional quenching of high frequencies due to the finite width of the electron beam. d is the actual noise floor.

Though equation (3) makes a lot of assumptions about the shape of the PSD at high frequencies, we only use this procedure to measure d. The value of d is not very sensitive to the exact form of the fit function, but we chose equation (3) because it can be physically justified.

3. NO VERTICAL ROUGHNESS

We first study the case without vertical roughness. We use the PSD of equation (2) with $\sigma = 1\,\text{nm}$, $\xi = 10\,\text{nm}$ and $H = 0.5$.

The measured PSD, for an infinitely narrow electron beam with 300 eV landing energy, is shown in figure 2a. It also shows the measurement of the noise floor using the fit of equation (3). Figure 2b shows the same PSD, with the noise floor subtracted. The measured PSD differs from the input PSD only in the very high frequencies. This divergence is most likely due to uncertainty in the noise floor measurement due to our choice of fitting function. We have run the same simulation with different electron beam landing energies (300 eV, 800 eV and 3000 eV). The results were practically indistinguishable from figure 2b. This implies that the high-frequency divergence in figure 2b is not due to the electron scattering cascade or material parameters.

In figures 2c and 2d, we use a more realistic Gaussian profile for the electron beam. The full width containing 50% of the current (FW50) is 3 nm, similar to current CD-SEMs. The effect of this finite spot size is a suppression of the PSD at higher frequencies. This can be modelled by convoluting the PSD of the line by the PSD of the spot. The blurring effect due to the finite spot size is a very dominant effect.

Because the effect of a finite electron beam spot size can be modelled well with a convolution, all future simulations in this work will be performed with an infinitely sharp beam.

4. ISOLATED LINES

We now also add roughness in the vertical direction according to equation (1). For simplicity, we consider isolated lines first, before going to dense lines & spaces in the next section.

We will use the following simplistic model to understand the results. A typical SEM signal is bright when the beam lands near a sharp edge, because electrons may escape from the side. We may expect that, when the beam

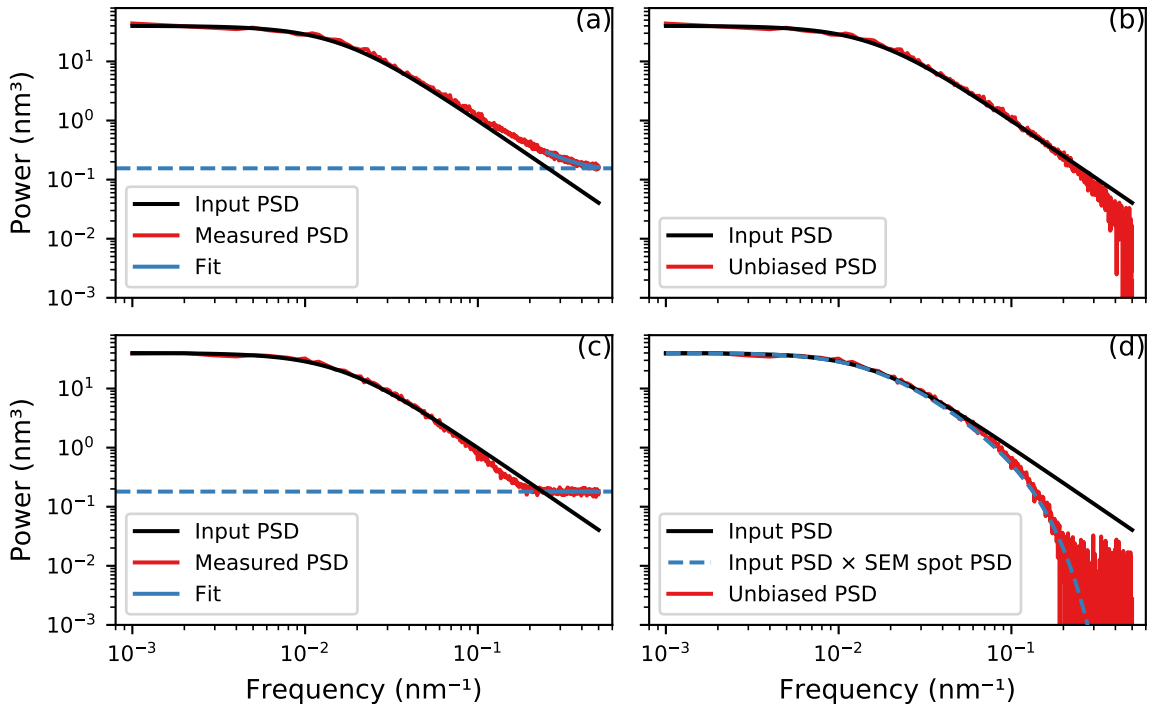

Figure 2. The input PSD (black curve) is compared to the PSD measured from simulated SEM images (red curves). There is no roughness in the vertical direction. The figures on the left show the measurement of the noise floor, the figures on the right show the result after noise floor subtraction. In (a) and (b) the electron beam is infinitely sharp; in (c) and (d) the electron beam has a Gaussian profile with 3 nm FW50. The dashed curve in (d) indicates the input PSD convoluted with the SEM spot.

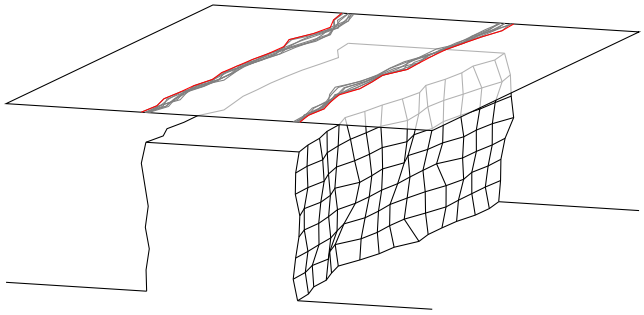

Figure 3. Illustration of the projection model. An example 3D rough line is shown. The contour of every slice of the geometry is projected onto the plane above the feature (grey lines). The red lines follow the outermost extrusions of the grey lines. The projection model assumes that the SEM observes this red line.

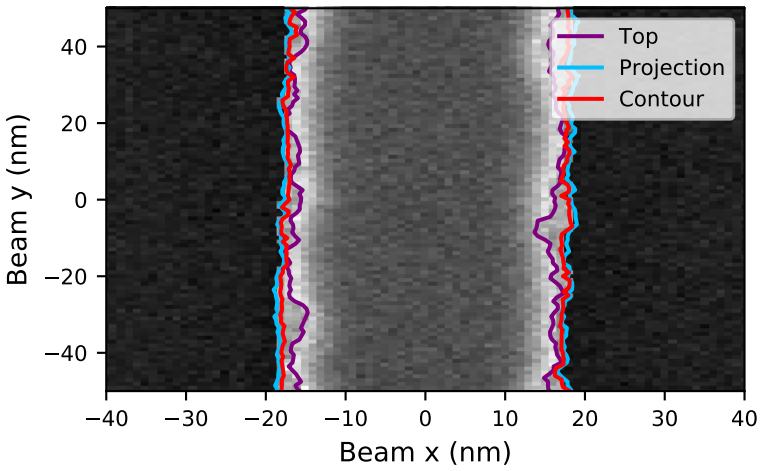

Figure 4. Typical SEM image of an isolated 3D rough line. The contour detected by the contouring algorithm (red curve), as well as the contour of the top slice (purple) and the projection model (blue) are overlaid. This is an 80 nm high line with $\sigma = 1\,\text{nm}$, $\xi_y = \xi_z = 10\,\text{nm}$, and $H = 0.5$.

lands on an extrusion on the rough sidewall, the SEM signal is also very bright. This means the SEM contour will go around all extrusions as seen from the top. We call this the "projection model", which is illustrated in figure 3.

Numerically, the projection model can be quantified by generating a random 3D rough sidewall. Then, at each position along the line, the maximum excursion in the vertical direction is taken. In this paper, we repeat this procedure for a very large number of sidewalls and find the average PSD. We have not been able to find an analytical expression.

The projection model gives a vertical averaging effect. If the correlation length in the vertical direction, ξ_z, is very large, the structure looks like there is no roughness in the vertical direction. Hence, the measured PSD will be similar to the PSD of a single slice of the structure. If ξ_z is very small, the projection model averages over many correlation lengths in the vertical direction. Hence, the observed mean edge position will shift outwards, and the roughness will be less than that of a single slice. The amount of averaging depends on the number of correlation lengths in the vertical direction: scaling both the height of the feature and ξ_z by the same factor gives the same final result.

A typical SEM image of an isolated 3D rough line is shown in figure 4. This figure also shows the contours detected by the contouring algorithm, the true contour of the top slice of the line, and the projection model's contour. By eye, it is clear that the projection model predicts the SEM contour quite well.

The accuracy of the projection model can be verified by comparing its predicted PSD to the measurement by the SEM. Such a comparison is shown in figure 5. The agreement between the projection model and the SEM measurement is excellent. The SEM measurement slightly underestimates the signal at very high frequencies, similarly to the situation of figure 2.

It is clear from figure 5 that the measured 3σ LER (given by the area below the blue curve), is biased significantly compared to the true 3σ SWR (given by the area below the black curve). This is consistent with the simulation and experimental studies mentioned in the introduction.[5,10–15]

Figure 6 shows the bias of measured 3σ values for a range of ξ_z/h, where h is the height of the feature. We have included the effect of the CD-SEM's spot size in this figure. The full SEM simulations were done with a Gaussian electron beam spot. The projection model was convolved with the appropriate spot PSD (as in figure 2). The agreement between the projection model and the full simulations is quite satisfactory.

Interpreted differently, figure 6 predicts that measured LER scales with film thickness if the on-wafer SWR is constant. This is a pure metrology effect. It is consistent with previous experimental observations,[28,29] where

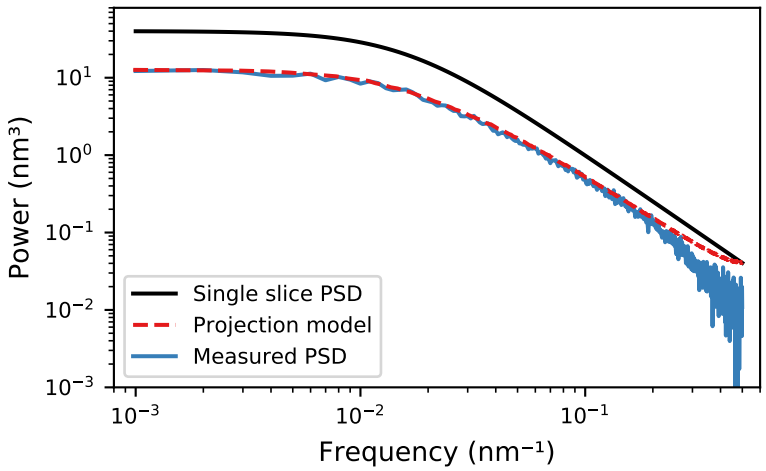

Figure 5. The input PSD of a single slice in the sidewall (black curve) is compared to the PSD predicted by the projection model (red) and the PSD measured by SEM (blue). This figure was made for the same parameters as figure 4.

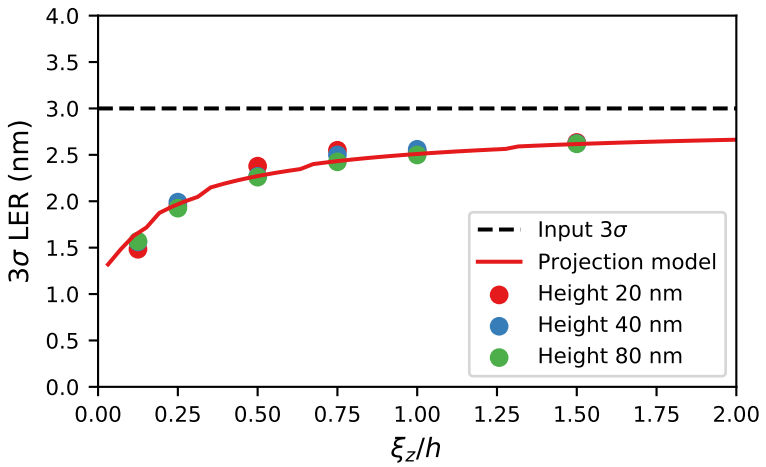

Figure 6. Comparing the bias in 3σ LER predicted by the projection model (solid curve) to observation from SEM images for a range of heights (points). The dashed black line indicates the true 3σ SWR. This figure was made for $\xi_y = 10\,\text{nm}$ and $H = 0.5$. A 3 nm FW50 Gaussian spot for the CD-SEM is included in these simulations.

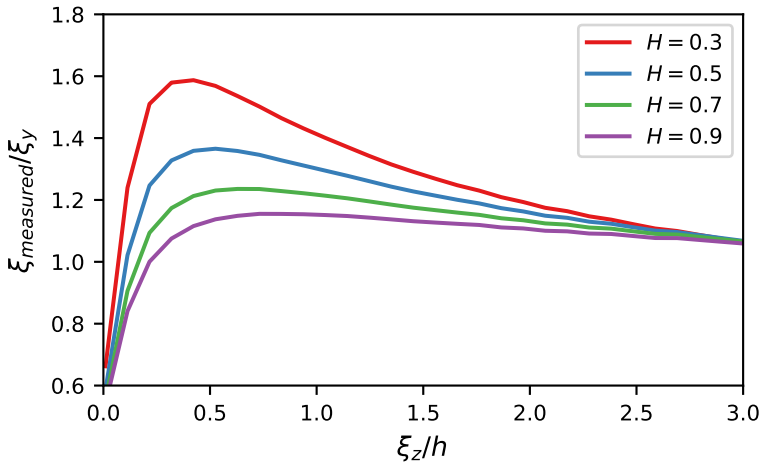

Figure 7. The bias in measured correlation length, for four different choices of Hurst exponent. The horizontal axis indicates the number of correlation lengths in the vertical direction. The vertical axis shows the measured correlation length, relative to the true correlation length along the line. The lines are predictions from the projection model, full SEM simulations are not shown.

LER is seen to increase as resist thicknesses are reduced. It is possible that a similar metrology component plays a role in those experimental studies, in addition to any change in on-wafer roughness.

As shown by Verduin *et al.*,[15] the correlation length measured by CD-SEM is biased if there is roughness in the vertical direction. We quantify this effect in figure 7. According to the projection model, only the ratio $\xi_{measured}/\xi_y$ is biased: scaling ξ_y results in a scaling of the PSD to lower or higher frequencies, while the shape is preserved.

The bias in measured correlation length shows an interesting trend. If there are many correlation lengths in the vertical direction (small ξ_z/h), the measured correlation length is significantly smaller than the true correlation length in the horizontal direction. When the structure is approximately two correlation lengths high, the measured correlation length peaks at a larger value than the true correlation length in the horizontal direction. For large ξ_z/h, the situation becomes similar to the case when there is no vertical roughness, and the bias disappears.

It can be seen in figure 5 that the projection model gives a lower Hurst exponent than the input PSD. We quantify this bias in figure 8 by numerically evaluating the projection model. The bias is almost linear, but it depends on ξ_z/h. The fact that the bias decreases as ξ_z/h increases is expected, as an absence of vertical roughness should make the measured PSD equal the input PSD.

We conclude this section by restating that the projection model predicts the SEM contour and its PSD very well for isolated lines. The projection model follows from purely geometrical arguments. This makes it very simple to understand and quantify. We did not attempt to find an analytical expression for the projection model PSD, but it is computationally very cheap to find numerical approximations by brute-force Monte Carlo simulation. This enables building a large library to translate "projected PSDs" back to the true sidewall PSD.

5. DENSE LINES AND SPACES

We are now interested in the more common situation of a dense pattern with 50% lines and 50% spaces. An example SEM image is shown in figure 9.

Comparing figure 9 to 4, we observe that some parts of the sidewall are darker in the dense line-space pattern. It is likely that electrons escaping from lower layers of the structure are blocked by the neighbouring walls. As a result, those deeper layers show up darker in the SEM image. The SEM contour is sensitive only to roughness which shows up brighter than the contouring threshold. Therefore, the projection model does not predict the SEM contour as well as it did for the case of purely isolated lines.

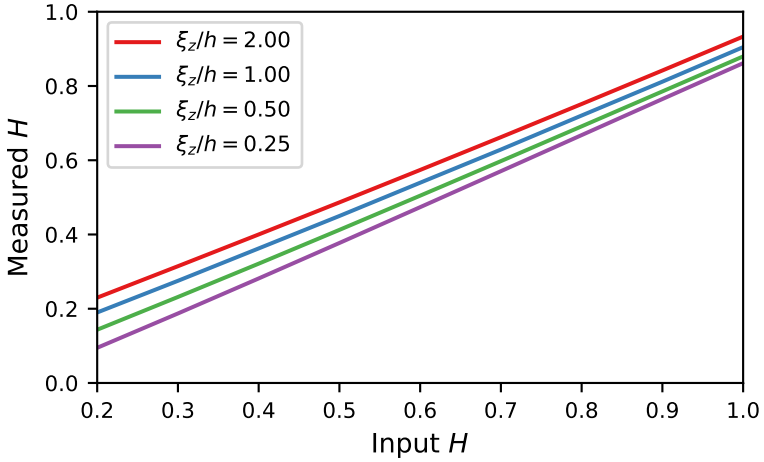

Figure 8. The bias in measured Hurst exponent, for four versions of correlation length in the vertical direction. The horizontal axis indicates the input Hurst exponent. The vertical axis shows the measured Hurst exponent. This data was obtained from the projection model, full simulation points are not shown.

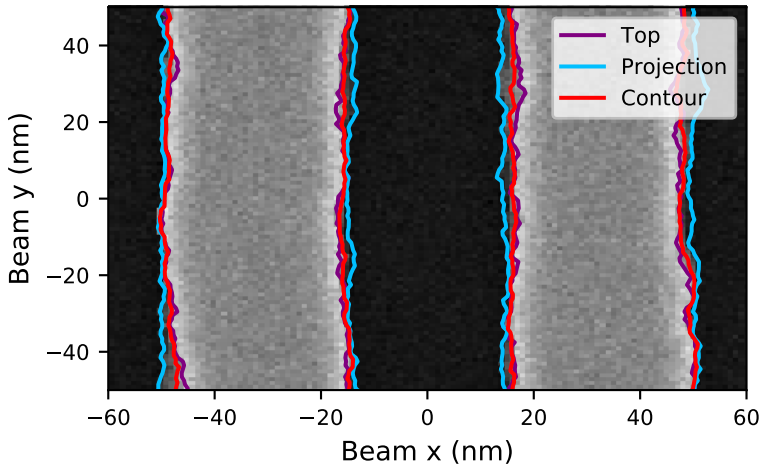

Figure 9. Same as figure 4, with trenches between the lines. The lines are 80 nm high, trenches are 32 nm wide.

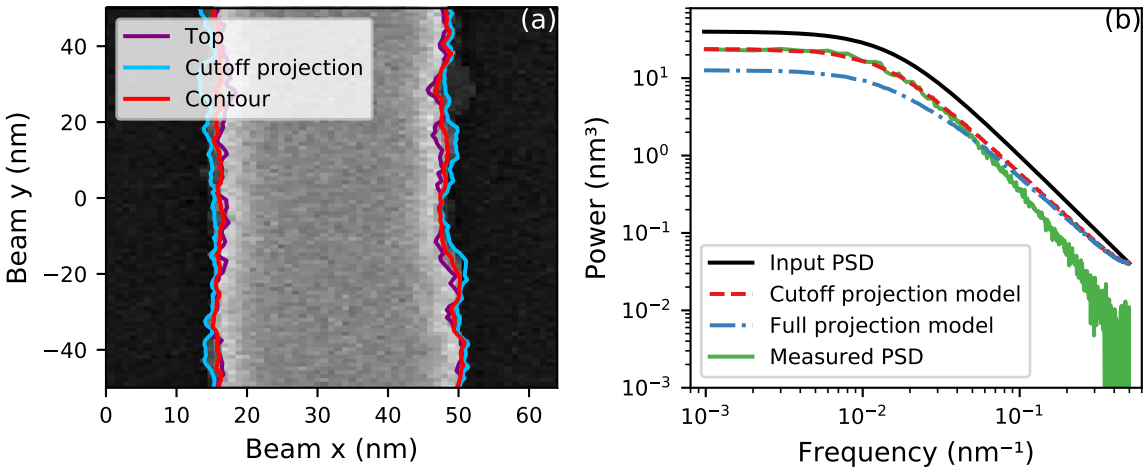

Figure 10. (a) Same as figure 9, but the light blue curve now shows the projection model with a cutoff at 30 nm depth. (b) Corresponding PSDs. The 30 nm cutoff depth was chosen to match the measured $PSD(0)$.

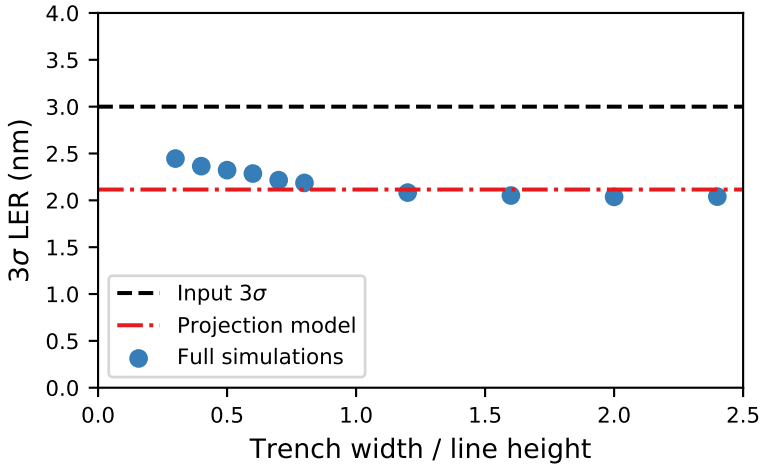

Figure 11. The bias in measured 3σ LER as a function of trench width. These simulations were done for 40 nm high lines, with $\xi_y = \xi_z = 10\,\text{nm}$ and $H = 0.5$.

As a first approximation, we may assume that the SEM is sensitive to roughness up to a certain "cutoff depth". We therefore investigate a "cutoff projection model", which assumes that the SEM contour follows the most extreme extrusion of the line above a certain depth. A typical result is shown in figure 10. This result was obtained by tuning the projection model's cutoff depth such that its low-frequency $PSD(0)$ matches the measured $PSD(0)$.

The match between model and measured PSDs in figure 10b is much worse than in figures 2 and 5. High frequencies are much more suppressed in the SEM image than the simple cutoff projection model predicts. The same is also clear from the real-space figure 10a, where the cutoff projection model does not follow the SEM contour very closely despite our efforts to match the PSDs. This indicates that the cutoff projection model is too simplistic.

The relation between the measured PSD and the contouring threshold is discussed in appendix A.

We now ask under what conditions lines can be considered "isolated enough" for the projection model (without cutoff) to be applicable. Figure 11 shows how the measured 3σ values evolve as trenches become wider. When the trench is wider than the feature height, the projection model predicts the measured 3σ value quite well. The projection model becomes worse as the trenches get narrower than the line height.

6. CONCLUSION

We have studied the influence of SWR on LER measured by top-down CD-SEM. This was done by generating features with known SWR, simulating corresponding CD-SEM images and measuring LER from those images.

We have verified that the popular method of PSD analysis works very well if the structures have no roughness in the vertical direction. The dominant factor limiting the measurement of the true on-wafer PSD is the electron beam's spot size. This causes a blurring effect, suppressing the PSD at high spatial frequencies.

If the structures are isolated and rough in the vertical direction, the CD-SEM observes the outermost extrusion over the full height of the structure. We believe that this simple geometrical interpretation will continue to work well for arbitrary feature shapes. We have verified it for trapezoids with a sidewall angle (see appendix A) and lines with roughness on the top (appendix B), but the general case needs further study.

As a result of this projection effect, the PSD measured by the SEM is biased significantly. Especially the 3σ LER, which is often considered the most important quantity, suffers heavily from this bias.

For dense lines and spaces, the situation is complicated by the fact that the SEM is less sensitive to the lower layers. If the trenches are as wide as, or wider than, the height of the lines, the SEM can still be seen to measure the outermost extrusion if the contouring threshold is low enough. Under those circumstances, the conclusions for isolated lines carry over to the dense case as the dense lines are "isolated enough". If the lines are higher than the trench width, we found no simple model that fully explains the SEM's behaviour. This is open for further research.

APPENDIX A. CONTOURING THRESHOLD

Throughout this paper, we have used a contouring threshold of 60%, a fairly common choice in industry. Most of our results are not sensitive to the choice of contouring threshold, except two situations.

A.1 Sidewall Angle

When there is a sidewall angle, the projection model works well for isolated lines. One thing to note is that the contouring threshold should not be set too high.

Figure 12a shows a SEM linescan over a trapezoidal edge without any roughness. Figure 12b shows a SEM image of a line with a rough sidewall (as illustrated in figure 1). Setting the contouring threshold too high puts the contour on top of the sidewall rather than near the outermost edge. This also makes it very sensitive to noise.

A.2 Dense Lines and Spaces

As mentioned, lower layers of dense lines & spaces are darker in SEM images due to a shadowing effect from neighbouring lines. This effect can be seen in figure 9. By eye, it is clear that a lower contouring threshold will put the SEM contour closer to the projection model.

We have kept the threshold at a constant 60% in the main part of this study. Given that deeper sidewall extrusions are darker than those near the top, one may expect that the projection model becomes more applicable when the contouring threshold is lowered.

Typical PSDs are shown in figure 13 for various contouring thresholds. As the contouring threshold is lowered, the measured PSD becomes more similar to the projection model: the PSD at low frequencies decreases while the PSD at high frequencies increases.

However, even at a very low 20% contouring threshold, the difference remains obvious. It is conceivable that an even lower contouring threshold will eventually match the projection model. If so, this will not be a practically useful limit because such extreme contouring thresholds are very sensitive to SEM noise.

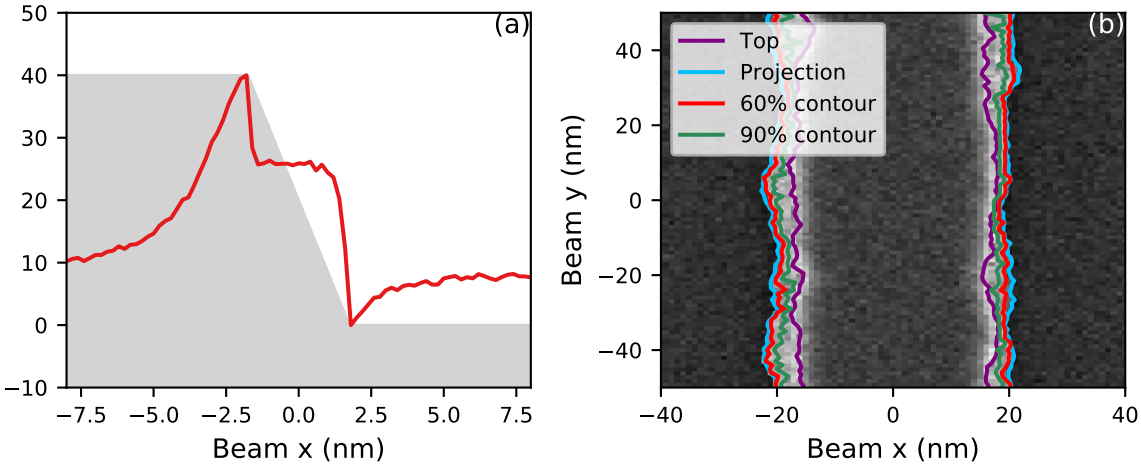

Figure 12. SEM images of isolated trapezoidal structures, 40 nm high and with an 85° sidewall angle. (a) SEM linescan over a structure without any roughness. The shaded area represents the shape of the structure. (b) SEM image of an isolated 3D rough line. The red and green curves show the measured contour lines at different threshold settings. The roughness parameters are the same as in figure 4.

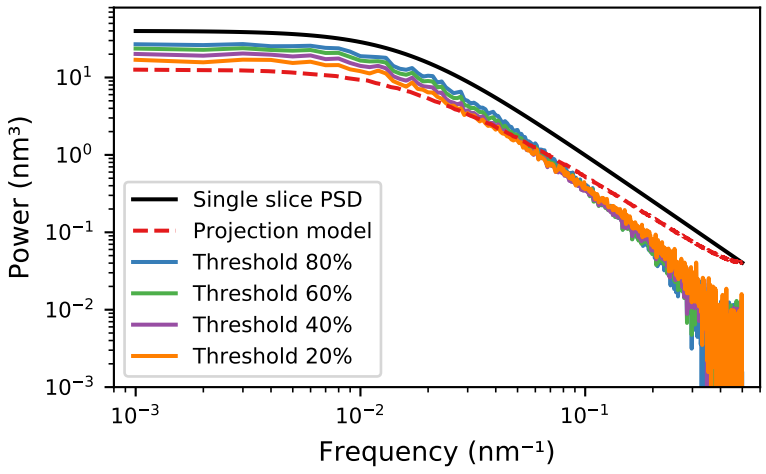

Figure 13. Measured PSDs for various contouring thresholds in dense lines & spaces. Physical parameters are the same as in figure 10.

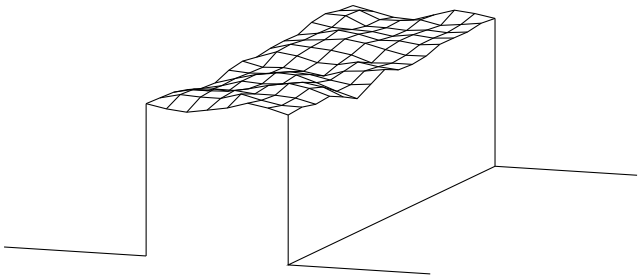

Figure 14. Sketch of the line profile studied in appendix B. We study lines with perfectly straight and vertical sidewalls. The top of the resist is modulated by a roughness model.

APPENDIX B. TOP ROUGHNESS

Resist features have roughness everywhere, not only along the sidewall. The projection model predicts that roughness on the top of the resist does not influence the measured LER. It is good to verify this.

We study resist lines with roughness only on the top, as illustrated in figure 14. The sidewalls are now flat, the sidewall angle is 90°. If the projection model is correct, the SEM contour is pure white noise. The roughness on top of the feature is described by the same PSD as before, equation (1), with $\sigma = 1\,\mathrm{nm}$, $\xi_x = \xi_y = 10\,\mathrm{nm}$ and $H = 0.5$.

Simulation results are shown in figure 15. The figures on the left show contoured SEM images, the figures on the right show the measured PSDs. The noise floor was not subtracted from the measured PSDs. The measured PSDs are almost flat, but not perfectly.

We have the following explanation for this effect. The top roughness is clearly visible in the SEM images. Because of this, the brightness of the line edges is also modulated. The brightness of the substrate is (on average) constant. The bright parts of the edge push the measured contour slightly outwards, hence the top roughness "leaks" into the measured LER. However, this effect is negligible compared to the usual power contained in LER signals (*cf.* figures 2, 5, 10). We estimate that the total variance due to non-white noise in figure 15b is $0.0014\,\mathrm{nm}^2$. In figure 15d, this is $0.011\,\mathrm{nm}^2$.

APPENDIX C. MATHEMATICAL DETAILS OF THE PSD

Roughness is often characterized in terms of the autocovariance function $R(x)$. A common choice is a stretched exponential,[30]

$$R(x) = \sigma^2 \exp\left(-\left|\frac{x}{\xi}\right|^{2\alpha}\right), \tag{4}$$

where α is the roughness exponent.

In this work, we have used the PSD of Palasantzas,[18] which corresponds to the following autocovariance function:

$$R(x) = \frac{2^{1-H}\sigma^2}{\Gamma(H)} \left|\frac{x}{\xi}\right|^H K_H\left(\left|\frac{x}{\xi}\right|\right). \tag{5}$$

$K_a(x)$ is the modified Bessel function of the second kind. If $H = 1/2$, this is identical to the autocovariance of equation (4) with $\alpha = 1/2$. For $H \neq 1/2$, equations (4) and (5) remain similar, with H taking the role of α. The main advantage of Palasantzas's choice is that the PSD has a known analytical form for all roughness exponents.

The 1D PSD, equation (2), can be obtained by Fourier transformation of equation (5):

$$PSD(f) = \int_{-\infty}^{\infty} \mathrm{d}x\, e^{-2\pi i f x} \frac{2^{1-H}\sigma^2}{\Gamma(H)} \left|\frac{x}{\xi}\right|^H K_H\left(\left|\frac{x}{\xi}\right|\right) \tag{6}$$

$$= \frac{\Gamma(H+1/2)}{\Gamma(H)} \frac{2\sqrt{\pi}\xi\sigma^2}{\left[1+(2\pi f\xi)^2\right]^{H+1/2}}. \tag{7}$$

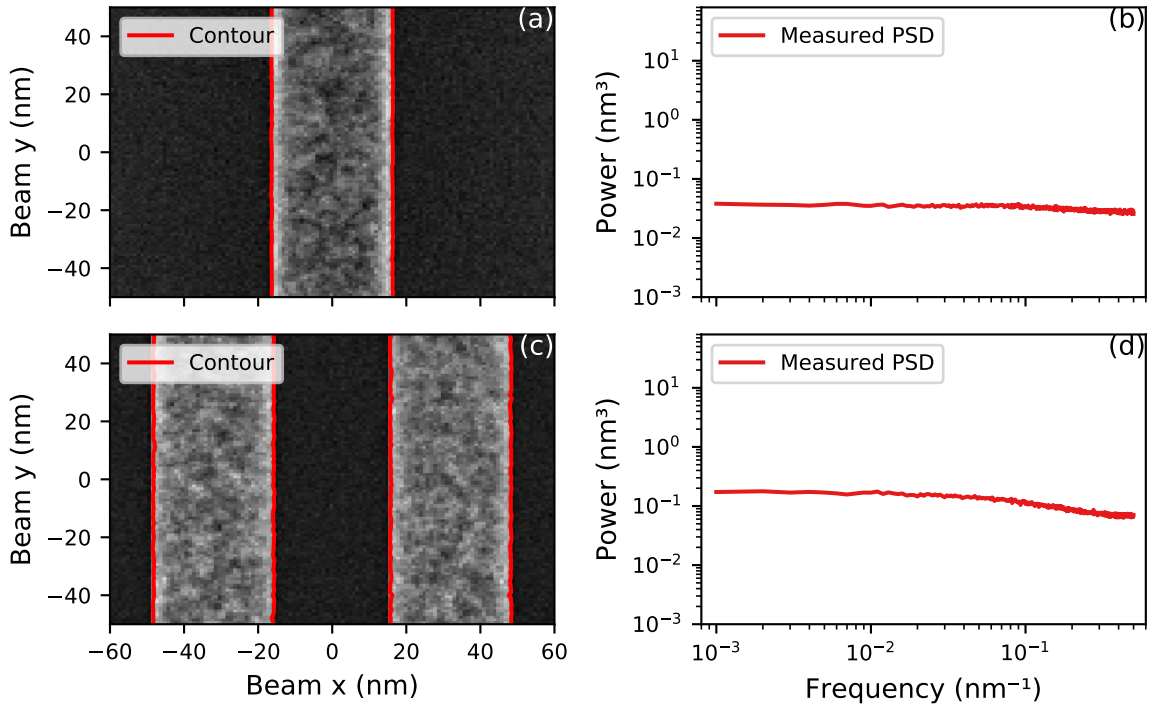

Figure 15. Simulated SEM images and measured PSDs for features with roughness on top of the lines only, as illustrated in figure 14. (a) and (b) are for isolated lines; (c) and (d) for dense lines & spaces. The noise floor was not subtracted from the measured PSDs in figures (b) and (d).

The 2D PSD can also be found from the autocovariance function of equation (5). To allow for different correlation lengths in the x and y directions, we replace $|x/\xi|$ by $\sqrt{(x/\xi_x)^2 + (y/\xi_y)^2}$:

$$R(x,y) = \frac{2^{1-H}\sigma^2}{\Gamma(H)} \left[\left(\frac{x}{\xi_x}\right)^2 + \left(\frac{y}{\xi_y}\right)^2 \right]^{H/2} K_H \left(\sqrt{\left(\frac{x}{\xi_x}\right)^2 + \left(\frac{y}{\xi_y}\right)^2} \right). \tag{8}$$

The 2D PSD, equation (1), can be obtained by 2D Fourier transformation:

$$PSD(f_x, f_y) = \int_{-\infty}^{\infty} \mathrm{d}x\, \mathrm{d}y\, e^{-2\pi i(f_x x + f_y y)}\, R(x,y) \tag{9}$$

$$= \frac{4\pi H \sigma^2 \xi_x \xi_y}{\left[1 + (2\pi f_x \xi_x)^2 + (2\pi f_y \xi_y)^2\right]^{H+1}}. \tag{10}$$

For $\xi_x = \xi_y$, this equation reduces to the original isotropic form in the work of Palasantzas.[18]

ACKNOWLEDGMENTS

We would like to thank Pieter Kruit (TU Delft) for valuable discussions.

REFERENCES

[1] Lorusso, G., Sutani, T., Rutigliani, V., van Roey, F., Moussa, A., Charley, A.-L., Mack, C., Naulleau, P., Constantoudis, V., Ikota, M., Ishimoto, T., and Koshihara, S., "The need for LWR metrology standardization: the imec roughness protocol," *Proceedings of SPIE* **10585**, 105850D (2018).

[2] Mack, C., "Systematic errors in the measurement of power spectral density," *Journal of Micro/Nanolithography, MEMS, and MOEMS* **12**(3), 033016 (2013).

[3] Hiraiwa, A. and Nishida, A., "Statistical- and image-noise effects on experimental spectrum of line-edge and line-width roughness," *Journal of Micro/Nanolithography, MEMS, and MOEMS* **9**(4), 041210 (2010).
[4] Goldfarb, D., Mahorowala, A., Gallatin, G., Petrillo, K., Temple, K., Angelopoulos, M., Rasgon, S., Sawin, H., Allen, S., Lawson, M., and Kwong, R., "Effect of thin-film imaging on line edge roughness transfer to underlayers during etch processes," *Journal of Vacuum Science & Technology B* **22**(2), 647–653 (2004).
[5] Foucher, J., Fabre, A., and Gautier, P., "CD-AFM versus CD-SEM for resist LER and LWR measurements," *Proceedings of SPIE* **6152**, 61520V (2006).
[6] Dahlen, G., Liu, H.-C., Osborn, M., Osborne, J., Tracy, B., and Del Rosario, A., "TEM validation of CD AFM image reconstruction: part II," *Proceedings of SPIE* **6922**, 69220K (2008).
[7] Kizu, R., Misumi, I., Hirai, A., and Gonda, S., "Accurate vertical sidewall measurement by a metrological tilting-AFM for reference metrology of line edge roughness," *Proceedings of SPIE* **10959**, 109592B (2019).
[8] George, S., Naulleau, P., Krishnamoorthy, A., Wu, Z., Rutter Jr, E., Kennedy, J., Xie, S., Flanigan, K., and Wallow, T., "Characterization of line-edge roughness (LER) propagation from resists: underlayer interfaces in ultrathin resist films," *Proceedings of SPIE* **7636**, 763605 (2010).
[9] Constantoudis, V., Kokkoris, G., Gogolides, E., Pargon, E., and Martin, M., "Effects of resist sidewall morphology on line-edge roughness reduction and transfer during etching: is the resist sidewall after development isotropic or anisotropic?," *Journal of Micro/Nanolithography, MEMS, and MOEMS* **9**(4), 041209 (2010).
[10] Foucher, J., Pikon, A., Andes, C., and Thackeray, J., "Impact of acid diffusion length on resist LER and LWR measured by CD-AFM and CD-SEM," *Proceedings of SPIE* **6518**, 65181Q (2007).
[11] Fouchier, M., Pargon, E., and Bardet, B., "An atomic force microscopy-based method for line edge roughness measurement," *Journal of Applied Physics* **113**(10), 104903 (2013).
[12] Fouchier, M., Pargon, E., and Bardet, B., "A new method based on AFM for the study of photoresist sidewall smoothening and LER transfer during gate patterning," *Proceedings of SPIE* **8685**, 86850B (2013).
[13] Lawson, R. and Henderson, C., "Understanding the relationship between true and measured resist feature critical dimension and line edge roughness using a detailed scanning electron microscopy simulator," *Journal of Vacuum Science & Technology B* **28**(6), C6H34–C6H39 (2010).
[14] Lawson, R. and Henderson, C., "Investigating SEM metrology effects using a detailed SEM simulation and stochastic resist model," *Proceedings of SPIE* **9424**, 94240K (2015).
[15] Verduin, T., Lokhorst, S., Kruit, P., and Hagen, C., "The effect of sidewall roughness on line edge roughness in top-down scanning electron microscopy images," *Proceedings of SPIE* **9424**, 942405 (2015).
[16] Thorsos, E., "The validity of the Kirchhoff approximation for rough surface scattering using a Gaussian roughness spectrum," *The Journal of the Acoustical Society of America* **83**(1), 78–92 (1988).
[17] Mack, C., "Generating random rough edges, surfaces, and volumes," *Applied Optics* **52**(7), 1472–1480 (2013).
[18] Palasantzas, G., "Roughness spectrum and surface width of self-affine fractal surfaces via the K-correlation model," *Physical Review B* **48**(19), 14472 (1993).
[19] Salvat, F., Jablonski, A., and Powell, C., "ELSEPA - dirac partial-wave calculation of elastic scattering of electrons and positrons by atoms, positive ions and molecules," *Computer Physics Communications* **165**(2), 157–190 (2005).
[20] Schreiber, E. and Fitting, H.-J., "Monte Carlo simulation of secondary electron emission from the insulator SiO2," *Journal of Electron Spectroscopy and Related Phenomena* **124**(1), 25–37 (2002).
[21] Palik, E., [*Handbook of Optical Constants of Solids, Five-Volume Set*], Elsevier (1997).
[22] Penn, D., "Electron mean-free-path calculations using a model dielectric function," *Physical Review B* **35**(2), 482–486 (1987).
[23] Shinotsuka, H., Tanuma, S., Powell, C., and Penn, D., "Calculations of electron stopping powers for 41 elemental solids over the 50 eV to 30 keV range with the full Penn algorithm," *Nuclear Instruments and Methods in Physics Research B* **270**(1), 75–92 (2012).
[24] Verduin, T., Lokhorst, S., and Hagen, C., "GPU accelerated Monte-Carlo simulation of SEM images for metrology," *Proceedings of SPIE* **9778**, 97780D (2016).
[25] Verduin, T., Kruit, P., and Hagen, C., "Determination of line edge roughness in low-dose top-down scanning electron microscopy images," *Journal of Micro/Nanolithography, MEMS, and MOEMS* **13**(3), 033009 (2014).

[26] Mack, C. and Bunday, B., "Using the analytical linescan model for SEM metrology," *Proceedings of SPIE* **10145**, 101451R (2017).

[27] Villarrubia, J. and Bunday, B., "Unbiased estimation of linewidth roughness," *Proceedings of SPIE* **5752**, 480–488 (2005).

[28] Putna, E., Younkin, T., Chandhok, M., and Frasure, K., "EUV lithography for 30nm half pitch and beyond: exploring resolution, sensitivity, and LWR tradeoffs," *Proceedings of SPIE* **7273**, 72731L (2009).

[29] van Look, L., Bekaert, J., Frommhold, A., Hendrickx, E., Rispens, G., and Schiffelers, G., "Optimization and stability of CD variability in pitch 40 nm contact holes on NXE:3300," *Proceedings of SPIE* **10809**, 108090M (2018).

[30] Sinha, S., Sirota, E., Garoff, S., and Stanley, H., "X-ray and neutron scattering from rough surfaces," *Physical Review B* **38**(4), 2297–2311 (1988).